Pseudo-Nonlinear Hydrodynamic Coefficients for Modelling Point Absorber Wave Energy Converters

Benjamin W. Schubert#1, Fantai Meng#2, Nataliia Y. Sergiienko#3, Will Robertson#4, Benjamin S. Cazzolato#5, Mergen H. Ghayesh#6, Ashkan Rafiee*7, Boyin Ding#8, Maziar Arjomandi#9

#*Ocean Wave Energy Research Group, School of Mechanical Engineering, The University of Adelaide South Australia, Australia, 5005*

1benjamin.schubert@adelaide.edu.au

**Carnegie Clean Energy limited, Perth, WA, Australia*

***Abstract*—This study presents dynamic simulation results of two point absorber wave energy converters comparing between linear, pseudo-nonlinear, and CFD models. When modelling wave energy converters, linear assumptions are commonly used to simplify calculations. One such assumption is that the hydrodynamic parameters do not change with pose. This study proposes the inclusion of position and orientation dependence in force estimation, specifically the hydrodynamic terms. A comparison between linear, the proposed pseudo-nonlinear, and CFD models show the effect of the linear assumption for cylindrical and spherical submerged buoys in three degrees of freedom, subject to regular waves. For the case of strong nonlinear hydrodynamic coupling between degrees of freedom, the linear and pseudo-nonlinear models are compared with published literature trends. Accounting for pose dependence of hydrodynamic forces, drag forces, and infinite frequency inertial effects showed trends closer to CFD results but with generally higher motion amplitudes. Significant differences in results for the cylinder are due to the presence of near-surface nonlinear effects that are not captured using linear potential flow solvers. Furthermore, a second order effect was observed in the results, suggesting the proposed method may be well suited to model sufficiently submerged buoys.**

***Index Terms*—Submerged point absorber, nonlinear hydrodynamics, numerical wave tank, wave energy converter, linear parameter varying**

I. Introduction

Wave energy converters (WEC), as a concept, have been developing for over two centuries [1]. As demand for power moves away from fossil-based fuels, research efforts have been intensifying since the 1970s. This enthusiasm has developed into a worldwide interest, leading to a number of technologies employing a variety of different operation principles [2]. Even with large interest globally, most devices are in the research and prototype stage [3]. For this technology to achieve economic viability for large scale energy production, a key area to develop for further study is modelling capability [4].

A common WEC design is a point absorber (PA), which is a device usually insensitive to wave direction. A typical cylindrical submerged point absorber is shown in Fig. 1. To model WECs, efficient and reliable computational methods are essential. Conventional modelling methods include linear boundary element method (BEM) solvers ANSYS AQWA [5], WAMIT [6], and NEMOH [7]. These solvers are used to calculate hydrodynamic parameters which are included in subsequent dynamic simulations. The more computationally intensive numerical wave tank (NWT) CFD approach, such as OpenFOAM or ANSYS Fluent, is becoming increasingly common in the industry. The BEM (also known as potential flow models) and NWT techniques represent linear and nonlinear approaches, respectively [1].

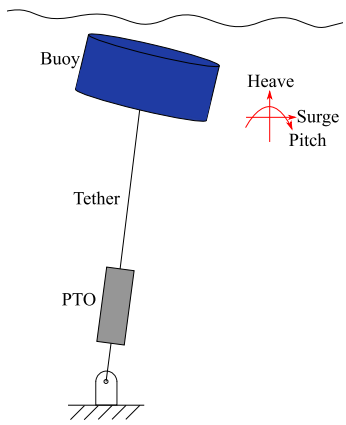

Fig. 1. A schematic of a single tether submerged cylindrical WEC displaying heave, pitch, and surge motions.

Linear BEM solvers provide fast solutions required for design optimisation studies. They do not account for changes in hydrodynamic coefficients as a function of geometric nonlinearities due to changes in pose, as the hydrodynamic coefficients are typically calculated around one position and orientation. Therefore, using results from linear BEM solvers cause the dynamic model to quickly lose accuracy as the motion amplitude of the buoy increases and nonlinearities become dominant [8].

Approaches to capture the nonlinear effects have been attempted previously by using extended linear solving methods,such as varying parameter model of a floating buoy with changing pitch [9]. Other models have involved recalculating the hydrodynamic parameters based on buoy wetted area at each time step for a floating spherical buoy [10] [11] and for a floating cylindrical buoy [11]. These models were constrained to move only in the heave direction. For submerged buoys,

the hydrodynamic parameters have a different dependence on depth and are independent of wetted area, which remains constant. Therefore, it is important to consider how hydrodynamic parameters change with both pitch and heave. Linear models for both floating and submerged buoys generally overestimate motion, and hence power [12], as the motion constraining effects of nonlinearities are ignored. As a whole, comparisons between linear and nonlinear modelling of submerged buoys remains largely unexplored and improvements in the current methods used may be needed to accurately model and rapidly develop these devices.

This paper explores the impact that pose has on the hydrodynamic coefficients and therefore the dynamics of two submerged point absorbers: (i) a cylinder, where coefficients are a function of position and orientation; (ii) a sphere, where coefficients are only a function of position.

Presented in this paper is a comparison between the motion characteristics of linear, pseudo-nonlinear, and fully nonlinear CFD models in three degrees of freedom (DOF) under regular (single frequency) waves. The linear model was constructed using the linear BEM solver NEMOH to find the hydrodynamic coefficients about a nominal position. The linear model does have geometric nonlinearities and drag forces but is referred to as linear in this study to reflect the method of calculating the hydrodynamic properties. The pseudo-nonlinear model used the same solver to find the hydrodynamic coefficients at a grid of points around the motion amplitude to provide linearly interpolated position-dependent hydrodynamic coefficients. Furthermore, the viscous drag force calculation incorporates velocity dependence on drag coefficients and basic orientation dependence. These coefficients and forces were used to investigate the nonlinear dynamics of the PA using MATLAB Simulink. An existing NWT in OpenFOAM was used to compare the linear and pseudo-nonlinear methods against CFD.

The mathematical model is presented in Section II. Included is the governing equation of motion and a description of each constituting term. An overview of typical linear assumptions is also provided for context. Section III discusses the implementation of the pseudo-nonlinear model and the simulation parameters. Section IV presents the results from the linear, pseudo-nonlinear, and CFD models subjected to regular waves. The results and implications on future modelling are discussed in Section V, with concluding remarks given in Section VI.

II. Mathematical Model of WEC

The schematic of the cylindrical buoy used in this study is shown in Fig. 1, with three DOF: surge, heave, and pitch, represented by

$$\mathbf{x} = \begin{pmatrix} \text{Surge} \\ \text{Heave} \\ \text{Pitch} \end{pmatrix} = \begin{pmatrix} x \\ z \\ \theta \end{pmatrix}. \tag{1}$$

Mathematically, the model can be represented by the governing equation, expressed as

$$\mathbf{M}\ddot{\mathbf{x}} = \mathbf{F}_\mathrm{e} + \mathbf{F}_\mathrm{r} + \mathbf{F}_\mathrm{h} + \mathbf{F}_\mathrm{pto} + \mathbf{F}_\mathrm{D} \ , \tag{2}$$

where $\mathbf{M}$ is the mass matrix containing the inertial terms for each DOF, given by

$$\mathbf{M} = \begin{bmatrix} m & 0 & 0 \\ 0 & m & 0 \\ 0 & 0 & I \end{bmatrix} \ , \tag{3}$$

with m being the mass of the buoy and I the moment of inertia about the centre of mass in the pitch direction.

The remaining terms $\mathbf{F}_\mathrm{e}$, $\mathbf{F}_\mathrm{r}$, $\mathbf{F}_\mathrm{h}$, $\mathbf{F}_\mathrm{pto}$, and $\mathbf{F}_\mathrm{D}$, are known as the excitation force, radiation force, hydrostatic or buoyancy force, power take off (PTO) force, and drag force respectively. Each of these terms, as well as how they may be estimated is discussed in the following sections, along with typical assumptions made to model them.

A. Excitation Force

The excitation force, $\mathbf{F}_\mathrm{e}$, from waves acting on the buoy is a function of input wave frequency, wave amplitude, buoy geometry, and buoy pose.

$$\mathbf{F}_\mathrm{e} = \mathbf{F}_\mathrm{e,amp} \sin(\omega t - \boldsymbol{\phi}) \ , \tag{4}$$

where $\mathbf{F}_\mathrm{e,amp}$ is the excitation force amplitude, and $\boldsymbol{\phi}$ is the excitation force phase vector. t represents time, and ω represents the wave frequency. The excitation force is the combination of the diffraction and Froud-Krylov forces [10].

B. Radiation Force

The radiation force, $\mathbf{F}_\mathrm{r}$, is the force applied to the buoy as it radiates waves as a result of motion. Radiation force is commonly represented in the time domain through the Cummins equation [13], given by

$$\mathbf{F}_\mathrm{r} = -\mathbf{A}_\infty \ddot{\mathbf{x}} - \int_0^t \mathbf{K}(t-t')\dot{\mathbf{x}}(t')dt' \ , \tag{5}$$

where $\mathbf{A}_\infty$ is the infinite frequency added mass and $\mathbf{K}$ is known as the memory function. This convolution integral represents the fluid memory affect in which the past state of the fluid effects the current state. In the frequency domain, the radiation force may be described as

$$\hat{\mathbf{F}}_\mathrm{r} = -[\mathbf{B}(\omega) + i\omega\mathbf{A}(\omega)]\hat{\dot{\mathbf{x}}}(i\omega), \tag{6}$$

where $\mathbf{B}(\omega)$ and $\mathbf{A}(\omega)$ is the frequency-dependent radiation damping and added mass respectively. In practice, within simulations, the radiation force is found using a well established method [14], involving constructing transfer functions from radiation damping and added mass with velocity as input and the integral in Equation (5) as the output [15]. For the purpose of these models, transfer functions of order five were found to appropriately fit the data.

C. Hydrostatic and PTO Forces

The hydrostatic force, $\mathbf{F}_\mathrm{h}$, acts only in the heave direction and PTO force, $\mathbf{F}_\mathrm{pto}$, is applied in the direction of the tether. Typically, for submerged buoys, there exists a pretension force provided by the PTO to counteract the hydrostatic force and give an equilibrium position below the surface of the

water [16]. For this study, the PTO force is considered to be a simple spring-damper arrangement,

$$\mathbf{F}_{\text{pto}} = \mathbf{T}(-b\Delta\dot{l} - k\Delta l - |\mathbf{F}_{\text{h}}|) \ , \tag{7}$$

where b and k are the damping coefficients and spring constants of the PTO respectively. The extension of the tether is represented by Δl. These parameters greatly impact the dynamics, and therefore the total power generated by the device. A transform, $\mathbf{T}$, converts the PTO force to the conventional 3 DOF [16].

Both b and k can be optimised for a given frequency wave and buoy [17]. Accordingly, for the purpose of comparing between linear, pseudo-nonlinear, and fully nonlinear CFD, these values will be optimised for each frequency to compare optimal cases. Optimal values are approximately given by the following by assuming tether extension is primarily due to heave motion,

$$b_{\text{opt}} = B_z(\omega) \ , \qquad k_{\text{opt}} = \omega^2(m + A_z(\omega)) \ , \tag{8}$$

where the subscript z refers to the heave direction. In the simulations, the optimal conditions gave large motion amplitudes with part of the buoy breaching the surface. To avoid this, the amplitude was reduced by increasing the damping value while using the optimal PTO stiffness to allow the range of motion to match the sampling grid.

The resonance frequencies of submerged single tether buoys for surge and heave directions are well established [18]. The two resonances approximately overlap when the following stiffness condition is met;

$$k_{\text{pto,overlap}} = \frac{g(\rho V - m)(m + A_z(\omega))}{(l + a)(m + A_x(\omega))} \ , \tag{9}$$

where l is the length of the tether, a is the distance between the tether connection point on the buoy and the center of mass, g is the acceleration of gravity, ρ is the density of water, V is the buoy volume, and A_x and A_z are the added mass in surge and heave, respectively.

When resonances coincide there will be a strong nonlinear coupling between surge and heave. This one-to-one internal resonance condition will be used in this study to demonstrate the impact of including some nonlinearities within the models. The optimal stiffness will be used for comparison with CFD cases to show the impact on weakly nonlinear operating conditions.

To calculate the power generated, PTO nonlinearities are ignored and the simplified equation for instantaneous power is

$$P_{\text{inst}} = b\Delta\dot{l}^2 \ . \tag{10}$$

D. Drag Force

The drag force, $\mathbf{F}_{\text{D}}$, acting on the buoy is modelled as

$$\mathbf{F}_{\text{D}} = -\frac{1}{2}\mathbf{C}_{\text{D}}\rho\mathbf{A}_{\text{D}}|\dot{\mathbf{x}}_{\text{r}}|\dot{\mathbf{x}}_{\text{r}} \ , \tag{11}$$

where $\mathbf{C}_{\text{D}}$ and $\mathbf{A}_{\text{D}}$ are the coefficient of drag and characteristic area respectively, and $\dot{\mathbf{x}}_{\text{r}}$ is the relative velocity of the buoy with respect to the surrounding water. The values for $\mathbf{C}_{\text{D}}$ and $\mathbf{A}_{\text{D}}$ are fixed in the body frame but not the global Cartesian frame and remain approximately constant for a large range of Reynolds numbers [19].

E. Typical Assumptions

The aforementioned forces are complicated to model within the time domain without a number of simplifications and assumptions. Typical assumptions include that:

- the hydrodynamic parameters are independent of buoy pose,
- the coefficients of drag are constant, independent of pitch angle and velocity, the surrounding fluid is stationary, and
- the phase of the excitation force remains constant as the buoy changes surge location.

III. Implementation of Pseudo-Nonlinear Model

In this section, the assumptions listed in Section II-E are addressed in the development of a pseudo-nonlinear dynamic model. Hydrodynamic parameters were introduced in the form of gain-scheduled methods for the excitation force and infinite frequency added mass, and an LPV (linear parameter-varying) system for the radiation force. For the cylinder, these parameters were varied as a function of heave and pitch. For the sphere, only heave was varied as the coefficients are independent of pitch. The viscous drag force was calculated by including velocity dependence in the drag coefficient in the form of Reynolds number calculations. Additionally, for the cylinder, the drag force incorporated pitch dependence by transforming the flow into vector components. For the sphere, the drag force is independent of pitch angle due to symmetry. Excitation force phase change due to motion was implemented as a function of surge, discussed in Section III-C.

A. Hydrodynamic Parameter Position Dependence

Model behaviour is highly dependent on the hydrodynamic parameters ($\mathbf{F}_{\text{e}}$, $\mathbf{B}(\omega)$, $\mathbf{A}(\omega)$). It is therefore critical to investigate the validity of holding these parameters constant for given frequencies as the pose of the buoy changes. Here, the calculation of these parameters was performed using NEMOH, a linear BEM solver [20]. NEMOH provides the amplitude and phase of the excitation force, the hydrodynamic damping, and added mass for a particular buoy at a range of input wave frequencies. To incorporate position dependence, the amplitude and phase of the excitation force and the infinite frequency added mass were calculated through gain-scheduled methods within Simulink. These methods linearly interpolate between a three dimensional lookup table for the cylinder (using heave and pitch), and between a two dimensional lookup table for the sphere (using heave). The radiation force was implemented with an LPV block in Simulink. This block takes an array of state-space models containing a sampling grid, enabling interpolation between models for varying heave and pitch values as required. A block diagram showing the excitation force gain-scheduled method approach is shown in Fig. 2.

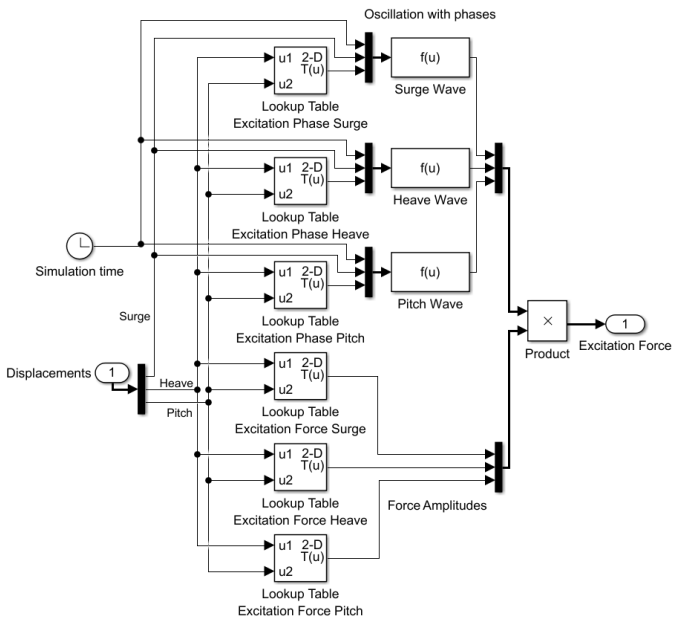

Fig. 2. Block diagram showing the excitation force gain-scheduled method approach. This details the flow of data used to find the interpolated force amplitudes for the cylinder. Force amplitudes for the spherical buoy did not use pitch values.

The range of motion for the cylinder involved varying heave position from -1.5m to 1.5m around the nominal position and pitch angle from $-10°$ to $10°$. For context, geometries of the buoys are provided on Table II. For both DOF, seven different positions and orientations were used, resulting in a sampling grid of 49 different poses. For the spherical buoy, due to symmetry, the pitch angle has no effect. Therefore, only the heave position was varied over the same range as the cylindrical buoy.

To summarise the methodology used for the proposed position-dependent hydrodynamic parameters, the following list shows the step by step procedure.

1) Specify heave and pitch positions
2) Use NEMOH to find $\mathbf{B}(\omega)$, $\mathbf{A}(\omega)$, $\mathbf{F}_{\text{e,amp}}$, and $\boldsymbol{\phi}$
3) Use $\mathbf{B}(\omega)$ and $\mathbf{A}(\omega)$ to create transfer functions describing how each DOF effects the radiation force in another DOF
4) Create a combined state-space for each pose
5) Combine state-space models into state-space array with sampling grid according to heave and pitch positions
6) Use the LPV block in Simulink to implement the state-space array
7) Specify $\mathbf{F}_{\text{e,amp}}$ and $\boldsymbol{\phi}$ into respective arrays and implement in Simulink using the Lookup Table block
8) Specify each element of $\mathbf{A}_\infty$ into respective arrays and implement in Simulink using the Lookup Table block

B. Drag Force Position Dependence

The viscous drag forces acting on the Sphere and Cylinder in the surge and heave directions were approximated through a similar gain-scheduled method. Firstly, the water velocity around the surge and heave positions were found using established theory [17]. The velocity of the buoys relative to the fluid was then used to calculate the Reynolds number at a given time step in each direction. This number was used to find a corresponding drag coefficient based on tabulated data [19]. In the spherical case, no viscous drag torque was modelled in the pitch direction due to symmetry. For the cylindrical buoy, the drag coefficient in the pitch direction was estimated from a previous study with a similar buoy [21]. The cylindrical buoy also has viscous drag forces which are pitch dependent. For an inclined cylinder, as a step towards including position dependence in the viscous drag force, the flow is divided into components in the axial direction of the cylinder, and perpendicular to the axial direction. The forces in the respective directions are found using the previously discussed method to estimate drag coefficients in the rotated reference frame. These forces are then rotated to align with the surge and heave directions. A block diagram showing the flow of data within the pseudo-nonlinear model of the spherical buoy is given in Fig. 3. Though this does not fully capture the nonlinearity of viscous drag, it is expected that this approach is a better representation of drag effects than if the drag coefficient is assumed to be constant and the pitch rotation of the cylinder was ignored.

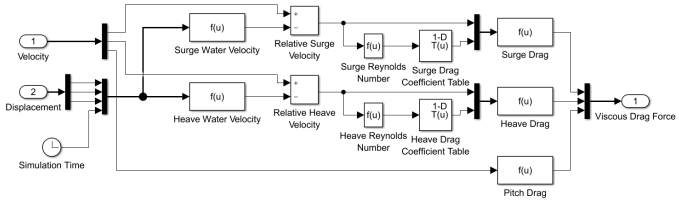

Fig. 3. Block diagram showing the viscous drag gain-scheduled method approach. This details the flow of data used to find the interpolated drag coefficients, and hence drag force amplitudes for the sphere. Force amplitudes for the cylindrical buoy change with pitch and are rotated accordingly.

C. Excitation Force Phase Position Dependence

The excitation force amplitude and phase provided by NEMOH is a description of the force experienced by the buoy at a nominal surge position. Therefore, as the buoy moves in the surge direction, the force experienced by the buoy should reflect this new position. The excitation force is described in Equation (4). The phase change due to surge position (ϕ_{s}) can be represented in the context of the excitation force by

$$\mathbf{F}_{\text{e}} = \mathbf{F}_{\text{e,amp}} \sin(\omega t - \boldsymbol{\phi} + \phi_{\text{s}}) \ , \tag{12}$$

where the phase change from surge is

$$\phi_{\text{s}} = kx \ , \tag{13}$$

and k is the wave number, found as the solution to [22]

$$\omega^2 = gk \tanh(kh) \ , \tag{14}$$

where h is the water depth.

D. Partially-Nonlinear Models from Literature

Previous work has included recalculating the excitation forces at each time step [11] based on the instantaneous wetted area of a floating buoy. This approach still uses a linear model for the radiation force and does not include drag forces. Additionally, the WECs were restricted to oscillate only in the heave direction. A similar study [10] calculated the excitation force at each time step based on instantaneous wetted surface, and uses a second order approximation of the diffraction and radiation force. This model also ignored viscous drag forces, was constrained to move vertically, and only simulated a single regular wave. Such techniques are common in partially-nonlinear models. Nonlinearity in the excitation force is expected to be the most influencial nonlinearity within PA WEC systems [2]. Comparatively, the radiation and diffraction forces require far more computational effort and have less impact on results.

One study, closer to the presented case, uses a Fully Nonlinear Potential Flow model on a submerged cylindrical buoy [23]. The submerged cylindrical buoy is restricted to two DOF, heave and surge. This nonlinear flow model effectively simulated two dimensional NWT results for limited scenarios, involving a small buoy and small wave amplitudes (cylinder with radius of 0.05m, and wave amplitude of 1.7cm). These limitations predispose the simulation to act in a regime in which linear assumptions provide reasonable results. While nonlinear potential flow models show promising results, further research is needed to quantify overall accuracy [2]. Additionally, such models are still computationally expensive compared to linear models [24].

Nonlinearities can have differing results for a change in simulated conditions [25]. One study, on submerged spherical buoys oscillating in the heave direction, showed that a weakly nonlinear model, based on the weak scatterer approximation, predicted lower amplitudes for some frequencies and higher for others [25]. Research in this area seems to indicate that nonlinearties impact models in differing ways and cannot be summarised as a simple increase or decrease compared to the linear model.

Another study which compares linear and nonlinear hydrodynamic parameters for cylinders [26] found that for cylinders close to the surface, the added mass and radiative damping in the heave and pitch directions differ significantly between linear and nonlinear simulations, whereas the surge direction remained relatively unchanged. Also shown in this study was that vortex shedding occurs on the edge of the cylinder, though this nonlinearity is expected to have minimal impact for the case presented. A more influential result seen in this study is the formation of a chute of water as the cylinder oscillates. We expect that this phenomenon could cause significant discrepancy between linear and nonlinear models.

The proposed pseudo-nonlinear method combines the nonlinear relationships present in hydrodynamic parameters as the pose varies, with the computational speed of linear modelling, and in three DOF. For the purpose of this study, the general trend of the responses at varying frequencies will be compared to investigate the degree to which nonlinearities are captured within the proposed model. Additionally, this model applies the same pseudo-nonlinear approach towards quantifying viscous drag effects, a force ignored in previous BEM studies.

E. Simulation Parameters

To compare the performance of each model, some common parameters were selected (Table I). In addition to the simulation parameters, the properties of the buoys and PTOs must be consistent between the respective models. These properties relating to the cylindrical and spherical buoys are presented in Table II.

TABLE I
SIMULATION PARAMETERS

Parameter	Value	Units
Acceleration of gravity, g	9.81	$\mathrm{m{\cdot}s^{-2}}$
Water density, ρ	1025	$\mathrm{kg{\cdot}m^{-3}}$
Kinematic viscosity of water, ν	1.004×10^{-6}	$\mathrm{m^2{\cdot}s^{-1}}$
Water depth, h	50	m
Submersion depth (buoy top), ds	2.5	m
Wave amplitude, A_w	0.5	m

TABLE II
BUOY PROPERTIES

Property	Value	Units
Cylinder radius, r_c	5	m
Cylinder height, h_c	5	m
Sphere radius, r_s	5	m
Buoy density, ρ_buoys	0.7ρ	$\mathrm{kg{\cdot}m^{-3}}$

For the linear and pseudo-nonlinear models, the viscous drag can only be approximated from literature values. In the linear case, the drag coefficients are assumed to be constant irrespective of surge and heave position. These coefficients of drag and the corresponding characteristic areas are given in Equations (15) and (16) where $\mathbf{C}_{\mathrm{D,\,c}}$, $\mathbf{A}_{\mathrm{D,\,c}}$, $\mathbf{C}_{\mathrm{D,\,s}}$, and $\mathbf{A}_{\mathrm{D,\,s}}$ are the coefficients of drag for the cylinder, characteristic area of the cylinder, coefficients of drag for the sphere, and the characteristic area of the sphere respectively [21].

$$\mathbf{C}_{\mathrm{D,\,c}} = \begin{pmatrix} 1 & 0 & 0 \\ 0 & 1.1 & 0 \\ 0 & 0 & 0.2 \end{pmatrix}, \mathbf{C}_{\mathrm{D,\,s}} = \begin{pmatrix} 0.5 & 0 & 0 \\ 0 & 0.5 & 0 \\ 0 & 0 & 0 \end{pmatrix} \tag{15}$$

$$\mathbf{A}_{\mathrm{D,\,c}} = \begin{pmatrix} hr_\mathrm{c}^2 & 0 & 0 \\ 0 & \pi r_\mathrm{c}^2 & 0 \\ 0 & 0 & (2r_\mathrm{c})^5 \end{pmatrix}, \mathbf{A}_{\mathrm{D,\,s}} = \begin{pmatrix} \pi r_\mathrm{s}^2 & 0 & 0 \\ 0 & \pi r_\mathrm{s}^2 & 0 \\ 0 & 0 & 0 \end{pmatrix}. \tag{16}$$

In the pseudo-nonlinear case, the drag coefficients for surge and heave are found by interpolating between tabulated results from literature [19], while the pitch drag coefficient is constant.

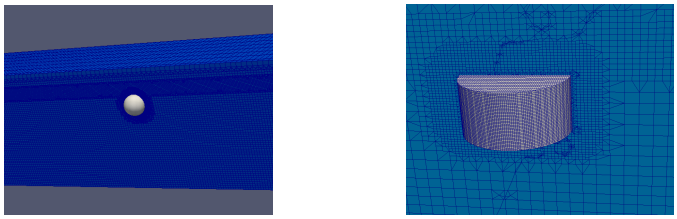

Fig. 4. A broad overview of the NWT is shown with the spherical buoy (left), and the cylindrical buoy mesh within the NWT (right).

For the fully nonlinear case, due to the computational resources required for this type of model, only five test cases were selected based on a distribution of periods. These five test cases, and the corresponding PTO parameters are given in Table III. The optimal PTO stiffness according to Equation (8) was used in these simulations. Test frequencies for the linear and pseudo-nonlinear model range from 0.1 to 2.5 rad/s.

TABLE III
CFD Test Cases

Period (s)	6	8	10	12	14
$K_{\text{pto,cylinder}}$ (MN·m^{-1})	1.07	0.62	0.38	0.25	0.17
$K_{\text{pto,sphere}}$ (MN·m^{-1})	0.79	0.46	0.29	0.20	0.14
$B_{\text{pto,buoys}}$ (MN·s·m^{-1})	0.14	0.14	0.14	0.14	0.14

F. CFD Setup

CFD models are nonlinear models used to simulate fluid structure interaction. They are computationally expensive but can be a powerful tool to acquire accurate simulated results. The CFD model was adapted from previous studies [12], [27]. A broad view of the numerical wave tank and a detailed view of the mesh surrounding the cylindrical buoy can be seen in Fig. 4. This model has been checked for convergence and has been validated against experimental data for spherical buoys.

IV. Results

A. Hydrodynamic results from NEMOH

Hydrodynamic parameters at a range of poses for the cylinder and sphere were found using NEMOH. Representative graphs of the added mass from Equation (6) for the cylindrical buoy at a heave position of 0.5m and varying pitch angles, and the added mass for the spherical buoy at varied heave positions are given in Figs 5 and 6, respectively. Radiation damping of the cylindrical and spherical buoys follow similar trends. Representative excitation forces and phases from Equation (4) are given in Figs 7 and 8 for the cylindrical and spherical buoys, respectively.

These added mass and damping coefficients were used to construct a model of the radiation force for different positions. However, for the spherical buoy, some terms fluctuate about zero due to numerical error or mesh imperfections. Additionally, the pitch-pitch and cross terms were expected to be zero

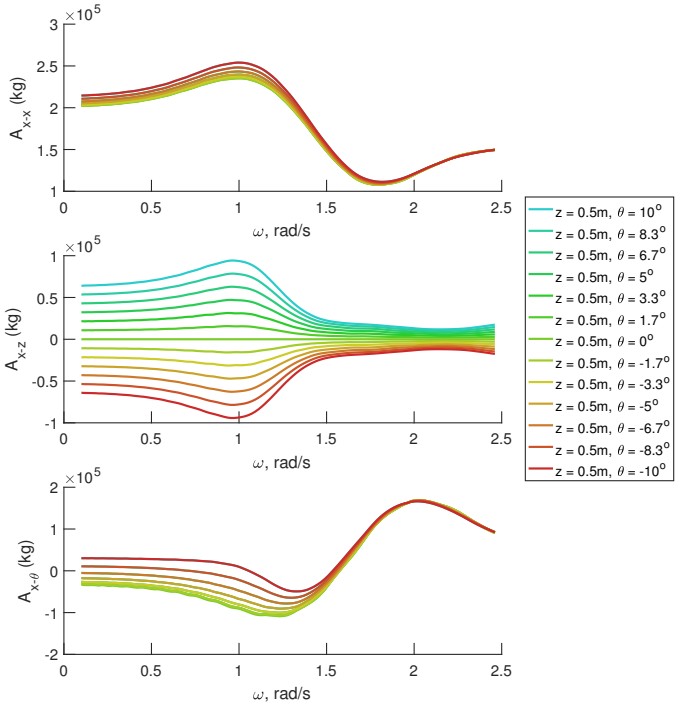

Fig. 5. Representative added mass values for the cylinder at constant surge and heave locations. Shown are the contributions to the added mass in the surge direction due to motions in all three DOF.

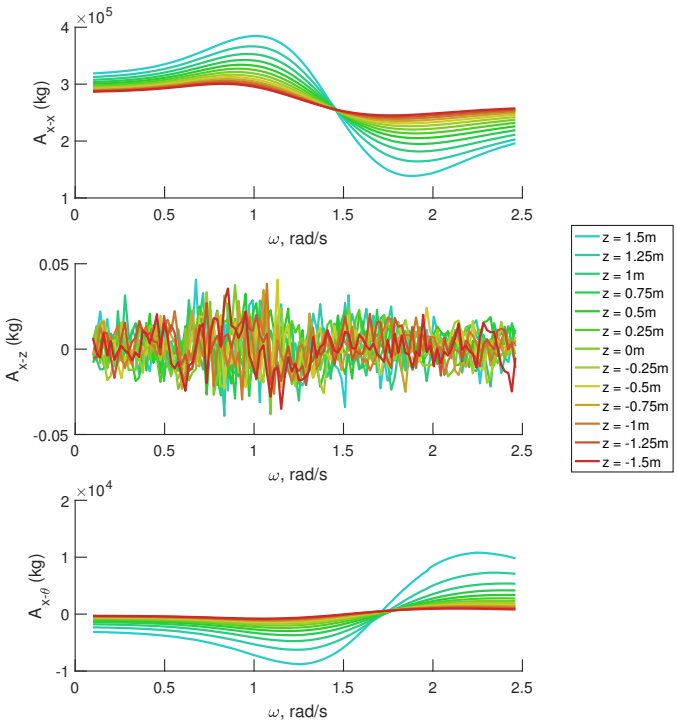

Fig. 6. Added mass values for the sphere at nominal surge location and pitch orientation. Shown are the contributions to the added mass in the surge direction due to motions in all three DOF.

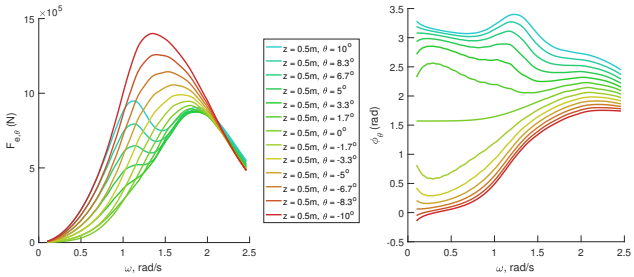

Fig. 7. Representative excitation forces (left) and phases (right) for the cylinder at nominal surge and heave locations. The excitation moment amplitude in the pitch DOF is shown.

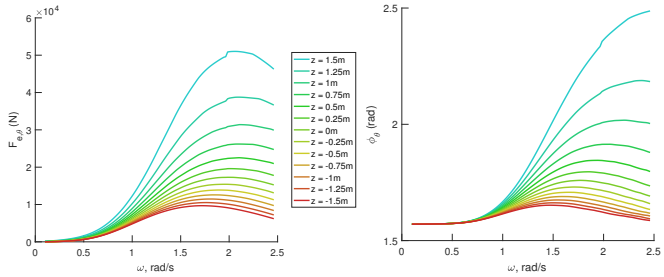

Fig. 8. Representative excitation forces (left) and phases (right) for the sphere at nominal surge location and pitch orientation. The excitation moment amplitude in the pitch DOF is shown.

but were found to be two orders of magnitude lower than surge-surge and heave-heave. These values are likely due to mesh imperfection and were also set to zero for the purpose of this study. Likewise, for the cylinder at the nominal pitch angle, the cross terms were near zero. These quantities were also set to zero in the calculation of transfer functions to prevent numerical artefacts in the radiation forces.

B. Simulation results in regular waves

In order to show the extent of the difference between the linear and pseudo-nonlinear models, the resonance frequency in heave was matched with the resonance frequency in surge using Equation (9). This provides large opportunity for strong nonlinear cross coupling effects. To isolate the effect of the hydrodynamic nonlinearity from viscous drag nonlinearity, the drag coefficient was held constant as with the linear simulations. In another set of simulations, the drag force was calculated according to the pseudo-nonlinear method with varying drag coefficient, (Fig. 9). This figure shows the oscillation amplitude for the cylinder when subjected to regular waves. A similar effect was also seen for the spherical buoy (not shown).

The linear, pseudo-nonlinear, and fully nonlinear models were subjected to simulated regular waves. Under this excitation, the steady state response of the WEC was recorded for each frequency. The mean of each DOF was found and used to center the signal for each DOF. A spectrum was obtained from this time domain signal using a Hamming window and a suitable frequency resolution. The maximum amplitude seen in each simulation was identified. The resulting peak oscillation

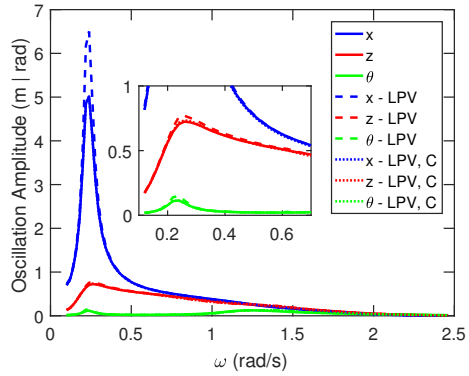

Fig. 9. The peak oscillation amplitude for the linear, pseudo-nonlinear (indicated by LPV), and pseudo-nonlinear with constant drag coefficient (indicated by LPV, C) models when the resonant frequencies in surge and heave are close. Results for the cylindrical buoy are shown.

in three DOF are presented in Figs 10 and 11 for the cylinder and sphere, respectively. The mean position of each buoy subjected to regular waves is shown in Figs 12 and 13 for the cylinder and sphere, respectively.

For practical WEC systems, another aspect to consider is the maximum PTO forces and power generated. The maximum PTO forces and the mean of the power generation were found at each frequency and displayed in Figs 14 and 15 for the cylinder and sphere, respectively.

V. Discussion

The simulated results show a notable difference between the linear and pseudo-nonlinear models. For the strongly coupled case with constant drag coefficients, the linear model and the pseudo-nonlinear models are approximately equivalent with the linear model overestimating and underestimating at different frequency ranges. However, when the drag coefficient is varied as a function of velocity, larger amplitudes are seen. This indicates the constant drag coefficients lead to an overestimate of drag forces. This finding informs the interpretation of subsequent results for the linear, pseudo-nonlinear, and fully nonlinear comparison. That is, larger motion amplitudes are expected for fully nonlinear results due to an overestimate in viscous drag forces in the linear model. Optimal stiffness conditions lead to increased motion amplitudes, which were used to further compare the linear, pseudo-nonlinear, and CFD approaches.

For the optimal stiffness condition, the heave oscillation amplitude of the pseudo-nonlinear model of the cylinder shows an increase around larger amplitudes and is relatively unchanged elsewhere compared to the linear model. A noticeable difference between the results is the change in mean positions about which the buoy oscillates. In both the strongly coupled and optimal stiffness PTO conditions, the pseudo-nonlinear approach resulted in larger displacements for the cylinder than for the spherical buoy. This is expected due to spherical symmetry preventing strong coupling between DOFs. This behaviour arises due to an asymmetric force experienced by the buoy over each oscillation cycle; that is, a net drift

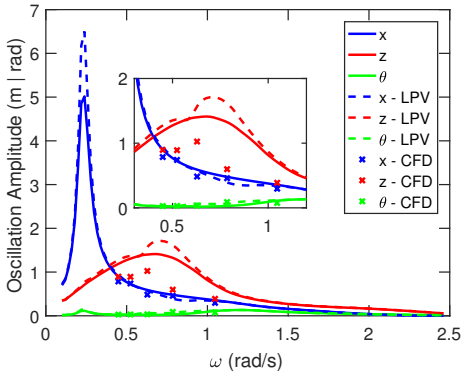

Fig. 10. The peak oscillation amplitude for the cylinder at various excitation frequencies when optimal PTO stiffness is used. The linear, pseudo-nonlinear (indicated by LPV), and fully nonlinear CFD results are shown.

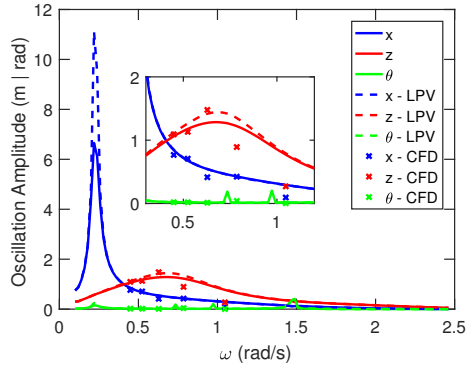

Fig. 11. The peak oscillation amplitude for the sphere at various excitation frequencies when optimal PTO stiffness is used. The linear, pseudo-nonlinear (indicated by LPV), and fully nonlinear CFD results are shown.

force. Drift forces are known to be a second order effect [28]. This behaviour is caused by a phase difference between the heave and surge excitation forces. This phase difference, coupled with the changing position of the buoy, creates a net movement in one direction until the stiffness force of the PTO is large enough to balance this drifting effect. The CFD results show the same bias trend though different peak locations and magnitudes for the spherical buoy. However, the mean position of the cylindrical buoy was clearly over-estimated in the pseudo-nonlinear method. One speculated result of this surge bias is that the tether extension is more coupled with rotation, allowing pitch to have more influence over power generation.

The difference between linear and pseudo-nonlinear oscillation amplitudes may, in part, be due to coupling between the three modelled DOF. This coupling can be seen in the hydrodynamic parameters in Fig. 5 for non-zero pitch angles. For the cylinder, pitch has a large effect on the effective added mass between surge and heave and pitch and heave motions. In the linear system, these cross terms are typically neglected as the pitch angle position is assumed to be zero. Conversely, the amplitude of oscillation of the spherical buoy is relatively unchanged for all DOF. Due to symmetry, the cross terms are zero and a changing heave location does not lead to strong hydrodynamic coupling. Consequently, less change between linear and nonlinear models is expected for spherical buoys.

The CFD results (Fig. 11) demonstrate that the linear model loses accuracy as the motion amplitude increases, agreeing with literature expectation. Results for the pseudo-nonlinear method do not clearly match CFD results but show a closer trend than the linear case, indicating that the LPV method captures some, but not all, nonlinearity in the hydrodynamics acting on the buoy. The trend for the sphere seems to be the peak thinning and a higher peak amplitude. The pseudo-nonlinear model results begin to show the same increase in peak amplitude. The pseudo-nonlinear model of the cylindrical buoy showed two distinct peaks, a large deviation from the linear model. Increased heave amplitudes occurred around the same frequencies as decreased surge amplitudes, indicating some degree of coupling between heave and surge. The CFD results for the cylinder again show that the pseudo-nonlinear results capture trends better than linear counterparts, though with greatly decreased amplitudes. The pseudo-nonlinear method gives larger amplitudes due to asymmetry in excitation forces in heave direction. That is, the exponential trend in excitation force indicates a greater increase for excitation force amplitude above the nominal position than decrease for below (Fig. 8). Therefore, nonlinearity in the excitation force is being captured. However, the motion amplitude is far less in the fully nonlinear CFD model (Fig. 10), indicating there is significant nonlinearity missing which the linear BEM hydrodynamic coefficients do not capture.

Other nonlinear forces acting on the buoy, such as overtopping or slamming, are not able to be modelled with linear BEM solvers. Submerged buoys, however, are away from highly nonlinear surface effects, and the outlined method does more closely approximate the nonlinearity of hydrodynamic forces than the simple linear BEM solver about a nominal position. It is commonly thought that the most influential nonlinearity for PA WEC systems is excitation force [2]. However, these results show that while the inclusion of nonlinearities in the excitation force does impact the results, there are more influential nonlinearties for this system not captured.

Linear BEM solvers are not able to fully capture the radiation forces for cylindrical buoys closer to the surface due to the formation of water jets and vortex shedding [26]. It was noticed that in the CFD simulations, significant vorticity was periodically occurring above the cylinder, indicating the presence of some complex resonance effect present in the column of water above the cylinder. Also, poor sampling grid resolution in the pseudo-nonlinear method and higher order nonlinear forces could be the reason for the discrepancy between pseudo-nonlinear and fully nonlinear results. Furthermore, interpreting the CFD results was made difficult due to the limited number of sampled frequencies. These reasons suggest that the proposed pseudo-nonlinear method is suited towards rapid modelling of submerged WEC devices only if additional improvements can be made which incorporate

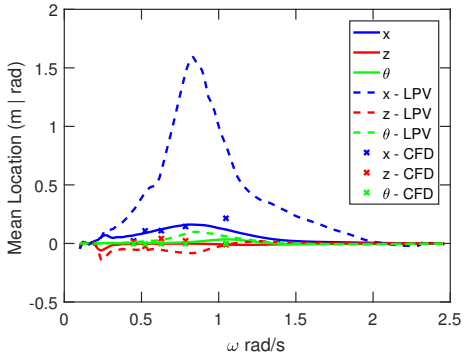

Fig. 12. The mean location for the cylinder at various excitation frequencies when optimal PTO stiffness is used. The linear, pseudo-nonlinear (indicated by LPV), and fully nonlinear CFD results are shown.

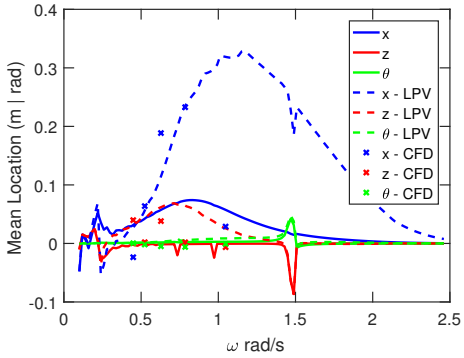

Fig. 13. The mean location for the sphere at various excitation frequencies when optimal PTO stiffness is used. The linear, pseudo-nonlinear (indicated by LPV), and fully nonlinear CFD results are shown.

nonlinear trends as buoys approach the surface. Alternatively, the proposed modelling method may be suited to specific operating conditions, such a sufficient submergence depth, because linear BEM solvers may adequately represent hydrodynamic parameters in particular conditions.

To comprehensively model WEC devices, it is important to accurately model the PTO forces. These forces influence installation cost and power generated. As an indication, the tether forces and power generated for all three modelling methods is provided in Section IV. These results show the pseudo-nonlinear method generally overestimates PTO forces and power generated. It should be emphasised that the viscous drag coefficient for the linear model is held constant and has been shown earlier to be the result of an over-estimated drag coefficient. However, as both the linear and pseudo-nonlinear model overestimate motion at higher frequencies, this is further evidence of the limitation that strong frequency-dependent nonlinearities are not captured using linear BEM solvers. One limitation of this study is that the CFD model was validated only against experimental data of spherical buoys, not cylindrical. Another limitation is that the results present the frequency of maximum oscillation amplitude seen in the response of the WECs when subjected to a regular wave, which does not account for harmonic distortions. Such harmonics were seen in the time domain results of CFD models, and, to a lesser extent, the pseudo-nonlinear model, particularly around natural frequencies.

Though the linear method proposed in this study has significant limitations, there are some benefits to such methods. The primary benefit of the linear and pseudo-nonlinear models is the drastic reduction in simulation time compared to CFD. The pseudo-nonlinear method is marginally more computationally expensive than the linear model. The linear method was able to simulate 2000 seconds in approximately 4 seconds, while the pseudo-nonlinear method took 10–15 seconds, on a standard computer. The CFD model simulated 300 seconds in approximately 2–3 days on a supercomputer. The found results and the potential benefits merit further investigation into the applicability of this modelling technique under a range of operating conditions. If the proposed pseudo-nonlinear model can be shown to capture significant nonlinearities in hydrodynamic forces, it can greatly speed up development of submerged WEC devices.

Further extensions of this research include improving the modelling method of the drag forces in each direction, which could be made more accurate by including drag coefficients of inclined cylinders rather than decomposing the flow direction into components. Furthermore, the resolution of the sampling grid of different positions and orientations may be increased to more adequately represent nonlinear trends in the hydrodynamic parameters. The model could be extended to explore the effect of larger wave amplitudes on submerged buoys. The CFD model could also be used to acquire results from more excitation frequencies to gain a clearer perspective of nonlinear effects over a broad range of operating conditions. Alternatively, the effect of surface nonlinearities in CFD could be further explored by varying the submergence depth. For submerged devices, this pseudo-nonlinear method presents a potential alternative to greatly improving simulation speed from CFD, while capturing some nonlinear behaviours arising from position dependant hydrodynamic parameters.

VI. Conclusion

In this study a linear, pseudo-nonlinear, and fully nonlinear hydrodynamic parameter model for two point absorbers were developed and the corresponding motion and forces were compared. The linear and pseudo-nonlinear models displayed similar motion amplitudes for a spherical buoy and differing amplitudes for a cylindrical buoy. The pseudo-nonlinear model incorporated position dependence into the hydrodynamic parameters and drag forces. The results showed increased nonlinear behaviour and more closely match the trend in the CFD results compared to linear methods. The proposed model demonstrated the ability to capture some higher order nonlinearities such as drift forces and nonlinear trends in excitation forces. The pseudo-nonlinear model showed only a small increase in computation time over the linear model, but showed some basic nonlinear behaviours noticed in the CFD results and matched the trend of the fully nonlinear results. The significant differences between the pseudo-nonlinear and

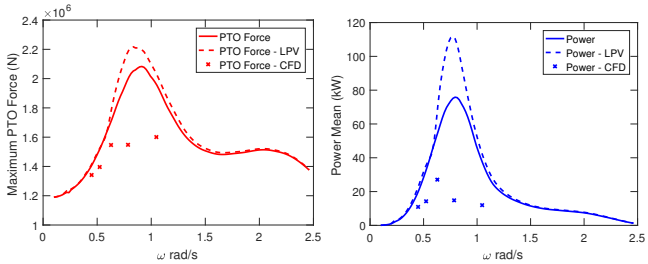

Fig. 14. The maximum PTO force (left) and mean of instantaneous power (right) experienced for each regular wave frequency for the cylindrical buoy.

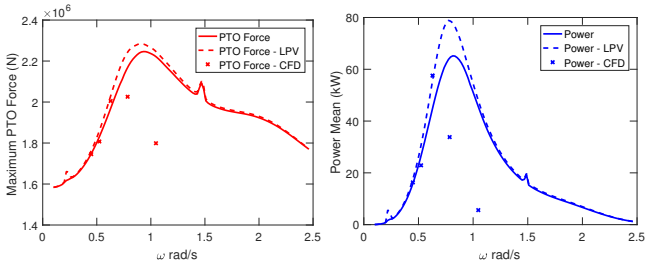

Fig. 15. The maximum PTO force (left) and mean of instantaneous power (right) experienced for each regular wave frequency for the spherical buoy.

fully nonlinear for the cylindrical buoy results suggest that nonlinearity in the hydrodynamic excitation forces are not the most significant nonlinearity for the buoy dynamics, and that the linear potential flow method for calculating hydrodynamic parameters becomes inadequate close to the surface. For the concept of submerged buoys, the results presented demonstrate the applicability of pseudo-nonlinear modelling for rapid simulation compared to fully nonlinear alternatives, and justify further investigation of this method.

Acknowledgement

This work was supported with supercomputing resources provided by the Phoenix HPC service at the University of Adelaide. This research has been supported by the Australian Government Research Training Program Scholarship.

References

[1] J. Cruz, *Ocean Wave Energy*, 1st ed. Springer-Verlag Berlin Heidelberg, 2008.

[2] M. Penalba, G. Giorgi, and J. V. Ringwood, "Mathematical modelling of wave energy converters: A review of nonlinear approaches," *Renewable and Sustainable Energy Reviews*, vol. 78, pp. 1188–1207, Oct. 2017.

[3] P. Hardy, B. Cazzolato, B. Ding, and Z. Prime, "A maximum capture width tracking controller for ocean wave energy converters in irregular waves," *Ocean Engineering*, vol. 121, pp. 516 – 529, 2016.

[4] J. Chozas, "International levelised cost of energy for ocean energy technologies an analysis of the development pathway and levelised cost of energy trajectories of wave, tidal and OTEC technologies," Ocean Energy Systems, Tech. Rep., May 2015.

[5] *AQWA User Manual*, ANSYS, Oct. 2012.

[6] *WAMIT USER MANUAL*, 7th ed., WAMIT Inc., 2016.

[7] A. Babarit, *NEMOH User manual*, Ecole Centrale de Nantes, Jan. 2014.

[8] J. Davidson, S. Giorgi, and J. V. Ringwood, "Linear parametric hydrodynamic models for ocean wave energy converters identified from numerical wave tank experiments," *Ocean Engineering*, vol. 103, pp. 31 – 39, 2015.

[9] A. McCabe, G. A. Aggidis, and T. Stallard, "A time-varying parameter model of a body oscillating in pitch," *Applied Ocean Research*, vol. 28, no. 6, pp. 359–370, 2006.

[10] A. Merigaud, J.-C. Gilloteaux, and J. V. Ringwood, "A nonlinear extension for linear boundary element methods in wave energy device modelling," in *Volume 4: Offshore Geotechnics; Ronald W. Yeung Honoring Symposium on Offshore and Ship Hydrodynamics*. ASME, Jul. 2012.

[11] M. Penalba Retes, A. Mérigaud, J.-C. Gilloteaux, and J. Ringwood, "Nonlinear Froude-Krylov force modelling for two heaving wave energy point absorbers," in *Proceedings of the 11th European Wave and Tidal Energy Conference*. European Wave and Tidal Energy Conference 2015, 2015.

[12] F. Meng, A. Rafiee, B. Cazzolato, B. Ding, M. Arjomandi, J. D. Piper, N. Sergiienko, and Q. Hu, "Numerical simulation of a submerged spherical point absorber with asymmetric mass distribution," in *Proceedings of the 11th European Wave and Tidal Energy Conference*, 2017.

[13] W. Cummins, "The impulse response function and ship motions," David Taylor Model Basin Washington DC, Tech. Rep., 1962.

[14] T. Perez and T. I. Fossen, "A Matlab toolbox for parametric identification of radiation-force models of ships and offshore structures," *Modeling, Identification and Control: A Norwegian Research Bulletin*, vol. 30, no. 1, pp. 1–15, 2009.

[15] R. G. Coe and D. L. Bull, "Nonlinear time-domain performance model for a wave energy converter in three dimensions," in *Oceans-St. John's, 2014*. IEEE, 2014, pp. 1–10.

[16] A. Babarit, J. Hals, M. Muliawan, A. Kurniawan, T. Moan, and J. Krokstad, "Numerical estimation of energy delivery from a selection of wave energy convertersfinal report," *Report, Ecole Centrale de Nantes & Norges Teknisk-Naturvitenskapelige Universitet*, 2011.

[17] J. Falnes, *Ocean waves and oscillating systems: linear interactions including wave-energy extraction*. Cambridge university press, 2002.

[18] F. Meng, B. Cazzolato, B. Ding, and M. Arjomandi, "Modal analysis of a submerged spherical point absorber with asymmetric mass distribution," *submitted to Renewable Energy*, 2017.

[19] R. D. Blevins, "Applied fluid dynamics handbook," *New York, Van Nostrand Reinhold Co., 1984, 568 p.*, 1984.

[20] M. Penalba, T. Kelly, and J. V. Ringwood, "Using NEMOH for modelling wave energy converters: A comparative study with WAMIT," *Centre for Ocean Energy Research (COER), Maynooth University, Co. Kildare, Ireland*, 2017.

[21] N. Y. Sergiienko, B. S. Cazzolato, B. Ding, and M. Arjomandi, "Three-tether axisymmetric wave energy converter: estimation of energy delivery," in *Proceedings of the 3rd Asian Wave and Tidal Energy Conference, Singapore*, 2016, pp. 163–171.

[22] S. Chao Jiang, Y. Gou, B. Teng, and D. Zhi Ning, "Analytical solution of a wave diffraction problem on a submerged cylinder," *Journal of Engineering Mechanics*, vol. 140, no. 1, pp. 225–232, Jan. 2014.

[23] E. Guerber, M. Benoit, S. Grilli, and C. Buvat, "Numerical modeling of fully nonlinear interactions of ocean waves with a submerged moving body," in *Proceedings of the 3rd International Conference on Ocean Energy. Bilbao, Spain*, 2010, pp. 1–6.

[24] L. Letournel, P. Ferrant, A. Babarit, G. Ducrozet, J. C. Harris, M. Benoit, and E. Dombre, "Comparison of fully nonlinear and weakly nonlinear potential flow solvers for the study of wave energy converters undergoing large amplitude motions," in *ASME 2014 33rd International Conference on Ocean, Offshore and Arctic Engineering*. American Society of Mechanical Engineers, 2014, pp. V09BT09A002–V09BT09A002.

[25] L. Letournel, C. Chauvigné, B. Gelly, A. Babarit, G. Ducrozet, and P. Ferrant, "Weakly nonlinear modeling of submerged wave energy converters," *Applied Ocean Research*, vol. 75, pp. 201–222, Jun. 2018.

[26] A. Rafiee and A. Valizadeh, "Nonlinear hydrodynamics of bluff bodies oscillating near freesurface," in *Proceedings of the twenty-eighth International Ocean and Polar Engineering Conference (ISOPE), Sapporo, Hokkaido, Japan*, Jun. 2018.

[27] A. Rafiee and J. Fiévez, "Numerical prediction of extreme loads on the CETO wave energy converter," in *Proceedings of the 11th European Wave and Tidal Energy Conference, Nantes, France*, 2015.

[28] B. W. Kim, S. Y. Hong, and H. G. Sung, "Comparison of drift force calculation methods in time domain analysis of moored bodies," *Ocean Engineering*, vol. 126, pp. 81–91, Nov. 2016.